Materials Advances

ROYAL SOCIETY OF CHEMISTRY

PAPER

View Article Online
View Journal

Cite this: DOI: 10.1039/d5ma00621j

Thermo-responsive single-chain cyclized/knotted polymers for cell encapsulation

Zhi Dou,*[a] Liangliang He,*[a] Wenxing Zhao,[a] Xiaoping Wang,[a] Hongyan Wang,[a] Jie Lu,[a] Chao Wang[b] and Liqiang Yang *[a]

Received 10th June 2025,
Accepted 2nd January 2026

DOI: 10.1039/d5ma00621j

rsc.li/materials-advances

Spinal cord injury (SCI) is a traumatic condition that results in the loss of motor and sensory functions. Mesenchymal stem cells (MSCs) have the potential to enhance the inflammatory microenvironment after SCI and promote nerve regeneration. However, maintaining long-term enrichment and sustained release of stem cells around the injured area remains a significant challenge. In this study, we synthesized a series of thermo-responsive single-chain cyclized/knotted polymers (SCKPs) using reversible addition–fragmentation chain transfer (RAFT) polymerization. By adjusting the types and ratios of monomers, we were able to tune the lower critical solution temperature (LCST) to approximately 37 °C. Importantly, SCKPs formed a half-interpenetrating polymer network (H-IPN) with thiolated hyaluronic acid (HA-SH), effectively encapsulating stem cells while maintaining high cell viability. This novel H-IPN shows great promise as a carrier for stem cell therapy in the treatment of SCI.

Introduction

Spinal cord injury (SCI) is a severe and incurable traumatic condition that often results in a significant loss of sensory and motor functions.[1,2] The initial mechanical trauma not only directly damages neurons but also triggers secondary injuries, such as inflammatory responses and oxidative stress, which worsen the condition.[1,3] Current clinical treatments, including surgical decompression and high-dose intravenous methylprednisolone, have limited effectiveness.[4,5] Surgery cannot restore neuronal damage or promote regeneration, and it carries inherent risks.[6] Long-term use of methylprednisolone may cause side effects such as osteoporosis and muscle atrophy, requiring careful dose management.[7–9] Although emerging therapies, like neurotrophic factors, can stimulate neuronal growth and survival, they require frequent high doses or repeated injections/implants, which may lead to immune rejection.[10,11] Therefore, traditional treatments often fail to substantially improve patient outcomes, and there is an urgent need to develop novel therapeutic strategies for SCI patients.

Adipose-derived mesenchymal stem cells (ADMSCs) have gained significant attention for SCI treatment due to their ease of isolation, low immunogenicity, and ability to secrete matrix components and factors that support tissue repair and neovascularization.[12–14] In recent years, ADMSCs have demonstrated anti-inflammatory and reparative properties, making them a promising option for SCI therapy.[15] However, the clinical effectiveness of local ADMSC injections is hampered by poor targeting and rapid degradation, limiting their therapeutic benefits.[16] To overcome these limitations, researchers have explored encapsulating ADMSCs using advanced biomaterials. Encapsulation provides a protective barrier that reduces immunogenicity, eliminating the need for immunosuppressants. These biomaterials mimic the extracellular matrix, enhancing the survival, differentiation, and function of encapsulated cells, while improving circulation time and cell targeting in damaged tissues.[17] This strategy significantly improves the therapeutic potential of SCI treatments by preventing the loss of stem cell function in the local microenvironment.

Currently, cell therapy primarily uses biodegradable hydrogel scaffolds, which offer a highly hydrated, elastic, tissue-like environment that is easy to manipulate and form *in vivo*.[18] However, these scaffolds often have drawbacks related to crosslinking efficiency, mechanical properties, and potential toxicity.[19,20] Single-chain cyclized/knotted polymers (SCKPs) are a new class of polymeric materials with a three-dimensional (3D) topological structure and multiple pendant vinyl groups, synthesized through the kinetically controlled radical polymerization of multivinyl monomers (MVMs).[21] Like other cyclic polymers, SCKPs exhibit favorable properties, including good solubility, a compact structure, high density, low intrinsic viscosity, low friction, a high glass transition temperature, high elasticity, reduced cytotoxicity, and increased circulation time.[21,22] These characteristics make SCKPs a promising candidate for cell encapsulation.

[a] Department of Pain Management, Xuanwu Hospital, Capital Medical University, Beijing, 100053, China. E-mail: yangliqiangxwpain@outlook.com
[b] Department of Pain Management, Xiong'an Xuanwu Hospital, Hebei, 070001, China

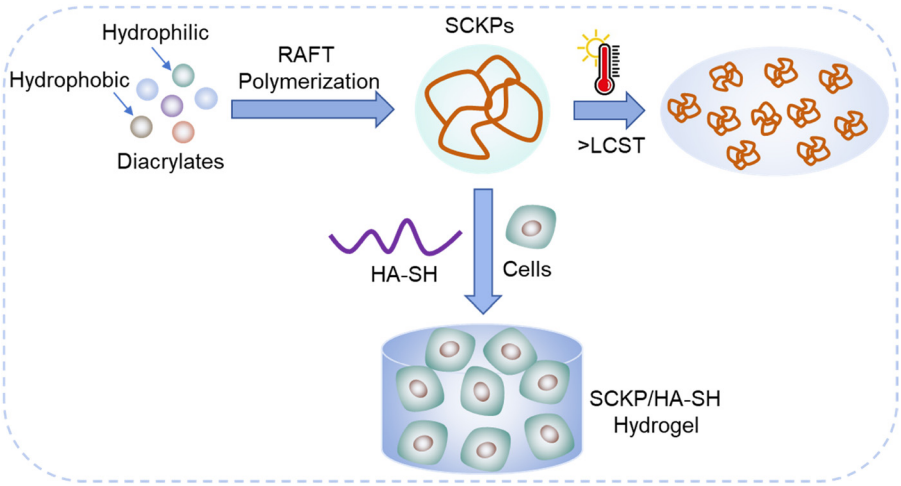

Scheme 1 SCKPs synthesized *via* RAFT polymerization exhibit thermo-responsiveness and can crosslink with HA-SH to form a hydrogel for *in situ* cell encapsulation.

In this study, we report the synthesis of thermo-responsive SCKPs *via* reversible addition–fragmentation chain transfer (RAFT) polymerization and the encapsulation of rat adipose-derived stem cells (rADSCs) (Scheme 1). By using monomers with varying amphiphilicity, including PEGDA, DEGDA, 2,2′-disulfonyl bis-(ethane-2,1-diyl) (DSDA), and dopamine methacrylamide (DMA),[23] we were able to fine-tune the lower critical solution temperature (LCST) of the SCKPs to approximate body temperature. Importantly, the optimized SCKPs crosslinked with thiolated hyaluronic acid (HA-SH) to form a half-interpenetrating polymer network (H-IPN), which effectively encapsulated ADMSCs *in situ* while maintaining high cell viability. SCKPs hold significant potential as a cell encapsulation platform for SCI cell therapy.

Materials and methods

Materials

Butanone was purchased from Alfa Aesar, while all other chemicals were sourced from Sigma-Aldrich (Arklow, Ireland) and used without further purification. Tetrahydrofuran (THF) was dried using Na_2SO_4 prior to use.

Monomer synthesis

2,2′-Disulfanediylbis(ethane-2,1-diyl) (DSDA) was synthesized by reacting bis(2-hydroxyethyl) disulfide with an excess of acryloyl chloride in a basic solvent (Fig. S1). In a 1000 mL round-bottom flask, 15.4 g (100 mmol) of bis(2-hydroxyethyl) disulfide and 37.5 mL (300 mmol) of triethylamine (TEA) were dissolved in 450 mL of THF. A solution of 24.4 mL (300 mmol) acryloyl chloride in 50 mL of THF was added dropwise over 2 hours with stirring at room temperature. The reaction was allowed to proceed for 24 hours at room temperature. The mixture was then filtered under vacuum to remove the precipitated TEA HCl, and the solvent was removed using rotary evaporation. The crude product was dissolved in 100 mL of dichloromethane and washed five times with 200 mL of 0.2 M Na_2CO_3 aqueous solution, followed by three washes with distilled water. The organic layer was dried with Na_2SO_4 and concentrated *via* rotary evaporation.

Dopamine methacrylamide (DMA) was synthesized by reacting methacrylic anhydride with dopamine hydrochloride in THF under alkaline conditions (Fig. S2). In a 1000 mL round-bottom flask, 30 g (78.66 mmol) of sodium tetraborate decahydrate and 12 g (142.69 mmol) of sodium bicarbonate were dissolved in 300 mL of distilled water. After bubbling argon through the solution for 20 minutes, 15 g (79.10 mmol) of dopamine hydrochloride was added. A second solution containing 14.1 mL (94.66 mmol) of methacrylic anhydride in 75 mL of THF was added dropwise. The pH was adjusted to 8.5, and the solution was stirred overnight. The DMA was purified by vacuum filtration, followed by two washes with 150 mL of ethyl acetate. The aqueous phase was acidified to pH 2 with 1 M HCl, making the product soluble in the organic phase. It was washed three times with 150 mL of ethyl acetate, dried over Na_2SO_4, and reduced to 80 mL by rotary evaporation. The product was precipitated into 800 mL of hexane and stored overnight at 4 °C to allow crystallization. The crystals were collected by vacuum filtration, redissolved in 100 mL of ethyl acetate, and precipitated again in 1000 mL of hexane. After another overnight storage at 4 °C, the crystals were filtered and dried overnight in a vacuum oven at room temperature.

Synthesis of SCKPs *via* RAFT copolymerization of MVMs

Single-chain cyclized/knotted polymers (SCKPs) were synthesized *via* reversible addition–fragmentation chain transfer (RAFT) polymerization. The monomer combinations and feed ratios are outlined in Table S1. Typically, in a 250 mL two-neck round-bottom flask, hydrophobic monomers poly(ethylene glycol) diacrylate (average molecular weight: 575 Da) (PEGDA575), diethylene glycol diacrylate (DEGDA) and DSDA, and hydrophilic monomers DMA and poly(ethylene glycol) diacrylate (average molecular weight: 700 Da) (PEGDA575) were dissolved in 0.1 M butanone. The chain transfer agent 2-cyanoprop-2-yl dithiobenzoate (CDB) and initiator 2,2′-azobis(2-methylpropionitrile)

(AIBN) were then added. After 30 minutes of argon bubbling to remove oxygen, the reaction mixture was stirred at 70 °C. The reaction progress was monitored using gel permeation chromatography (GPC) every hour. When the polydispersity index (PDI) reached approximately 1.5, the reaction was quenched by cooling with ice and exposing the mixture to air. The polymers were purified by precipitation in a mixture of hexane and diethyl ether (1 : 2 by weight). After 20 minutes of stirring, the solutions were allowed to stand for 30 minutes at −20 °C. They were then centrifuged at 4000 rpm and 4 °C for 20 minutes. The precipitated polymers were collected and dried in a vacuum oven.

GPC measurement

The number-average molecular weights (M_n), weight-average molecular weights (M_w), and PDI of the polymers were determined using GPC (Agilent 1260 Infinity II) equipped with a refractive index detector. The GPC columns (PolarGel-M Guard, 50 mm × 7.5 mm, and PolarGel-M, 300 mm × 7.5 mm) were eluted with dimethylformamide (DMF) containing 0.1% lithium bromide (LiBr) at a flow rate of 1 mL min^{-1} at 50 °C. Linear poly(methyl methacrylate) (PMMA) standards were used for calibration. Polymer samples (5–10 mg) were dissolved in 1 mL of DMF and filtered through a 0.22 μm filter prior to measurement.

Proton nuclear magnetic resonance (^{1}H NMR) characterisation

Samples (10 mg) were dissolved in 700 μL of deuterochloroform ($CDCl_3$) or deuterated dimethyl sulfoxide (d-DMSO). The ^{1}H NMR spectra were recorded using a 400 MHz JEOL NMR spectrometer with 32 scans. Data were processed using MestReNova software.

Measurement of lower critical solution temperature (LCST) of SCKPs

The optical transmittance of the SCKP solutions was measured at 350 nm using a UV-VIS spectrometer (SpectraMax M3 MultiMode Microplate Reader) at various temperatures ranging from 24 °C to 80 °C. The LCST was defined as the temperature at which the optical transmittance decreased by 50%. LCST measurements were performed for SCKPs at concentrations of 1 mg mL^{-1}, 5 mg mL^{-1}, and 10 mg mL^{-1} in pure water, phosphate-buffered saline (PBS), and Dulbecco's Modified Eagle Medium (DMEM).

Cell encapsulation with SCKPs

Cells were seeded at a density of 20 000 cells per well in a 96-well plate two days prior to encapsulation. SCKPs dissolved in DMEM at 1 mg mL^{-1} were added to the cell culture medium and heated to 37 °C. Images were taken before and after heating using an Olympus CK53 microscope.

Fabrication of SCKP/HA-SH hydrogels

Semi-IPN hydrogels were formed by crosslinking SCKPs with HA-SH. SCKPs (1 mg mL^{-1}) were incubated with the cells for 10 minutes, and the temperature was raised above the LCST. Then, 10 mg of HA-SH dissolved in 500 μL of Hank's buffer (2%) was added, and the plate was incubated for 30 minutes. Images were taken before and after SCKP addition and 30 minutes after HA-SH addition.

Measurement of cell viability

After two days of incubation with SCKPs at concentrations of 10, 50, and 100 μg mL^{-1} (n = 4), cell metabolic activity was measured using the alamarBlue assay. The cell culture medium was replaced with alamarBlue solution (10% dilution in DMEM), and the cells were incubated for an additional hour. Fluorescence was measured using a SpectraMax M3 MultiMode Microplate Reader.

Statistical analysis

Data were analyzed and plotted using SPSS 19.0 and GraphPad Prism 8.0. Results are presented as mean ± standard deviation (SD). Comparisons between two groups were made using Student's t-test.

Results and discussion

Synthesis of DSDA and DMA

The successful synthesis of DSDA and DMA monomers was confirmed using ^{1}H NMR spectroscopy. The ^{1}H NMR spectrum of the synthesized DSDA showed five characteristic signal peaks with corresponding chemical shifts and integration values: two triplets at δ 2.9 ppm and δ 4.4 ppm which are attributed to the methylene groups adjacent to the sulfur atoms, two doublets at δ 5.9 ppm and δ 6.4 ppm, corresponding to the protons on the carbons next to the carbonyl group, and a multiplet at δ 6.2 ppm assigned to the vinylic protons (Fig. S3). For DMA, the ^{1}H NMR spectrum revealed key significant signal peaks as follows: three singlets at δ 1.8 ppm, δ 5.2 ppm, and δ 5.6 ppm, two triplets at δ 2.5 ppm and δ 7.9 ppm, a quartet at δ 3.2 ppm, and a multiplet in the range of δ 6.6–6.4 ppm (Fig. S4).

Synthesis and characterization of SCKPs

To achieve thermo-responsiveness, particularly with an LCST near 37 °C, it is essential to carefully control the amphiphilicity of the SCKPs by selecting monomers with varying hydrophobicity and optimizing their feed ratios.[24,25] We selected PEGDA575, DEGDA, and DSDA as hydrophobic monomers, while PEGDA700 and DMA were chosen as hydrophilic monomers. These monomers were copolymerized through RAFT polymerization using different combinations and feed ratios[25] (Fig. 1a). To produce polymers with a cyclic/knotted topological structure while avoiding crosslinking, the feed ratio of the monomers to CDB and AIBN was fixed at 800 : 4 : 1,[26] with a monomer concentration of 0.1 M. The evolution of polymer PDI was monitored using GPC.[27] The reaction was stopped before the PDI approached 1.5 to prevent intermolecular polymer combination, which could result in insoluble polymers. In total, five soluble polymers were successfully synthesized, although the polymer containing DMA was insoluble.[28] The topological structure of the synthesized SCKPs was verified using the Mark–Houwink (M–H) plot.[29,30] Generally, an α value lower than 0.5 in the M–H plot indicates a 3D topological structure. The M–H plots for different SCKPs are

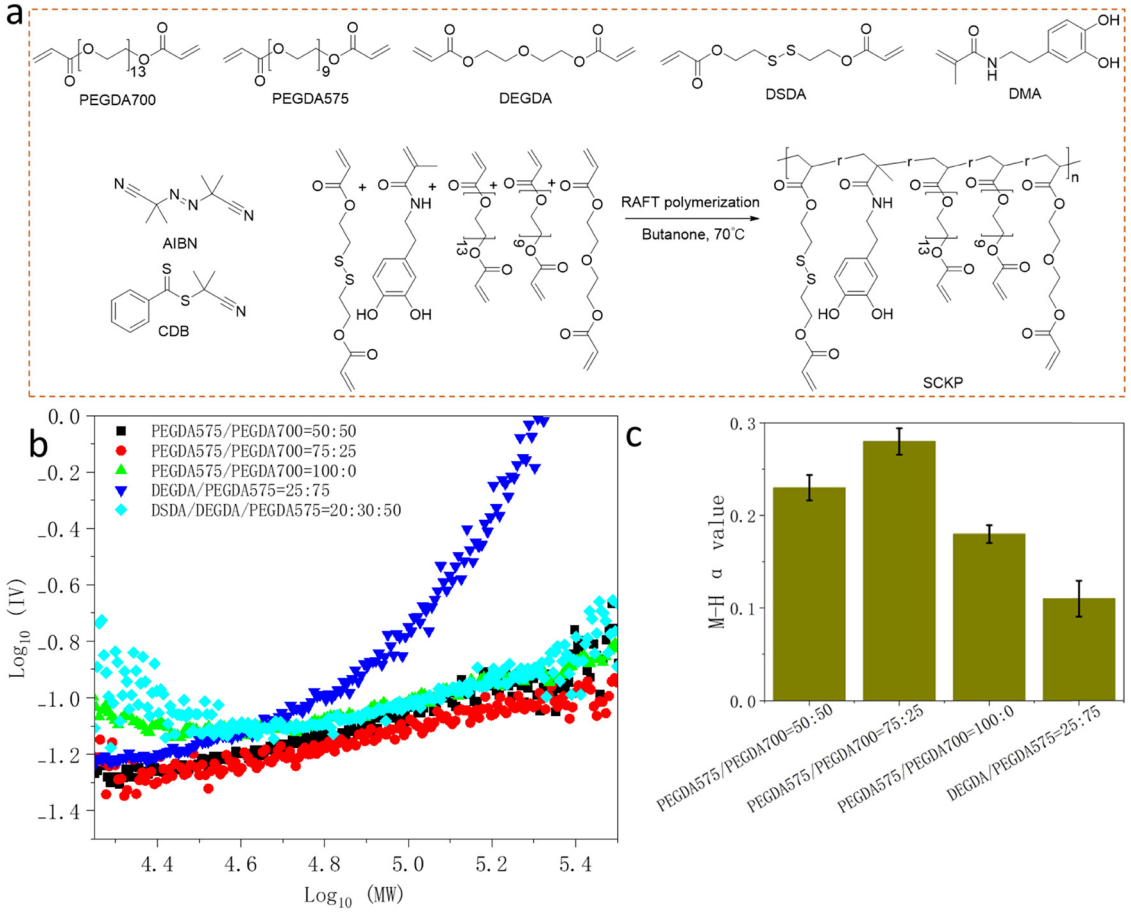

Fig. 1 Synthesis and characterization of SCKPs. (a) Monomer and multivinyl monomers are copolymerized *via* RAFT polymerization to synthesize SCKPs. (b) The Mark–Houwink (M–H) plots for various SCKPs. (c) The α values from the M–H plots for different SCKPs.

presented in Fig. 1b. For the SCKPs with a PEGDA575/PEGDA700 monomer combination at a 50 : 50 feed ratio, an α value of 0.23 was observed (Fig. 1c), suggesting a relatively compact coil conformation. When the feed ratio was adjusted to 75 : 25, a slightly higher α value of 0.28 was detected, indicating a more expanded conformation. Interestingly, when the monomer ratio shifted to 0 : 100 (without PEGDA575), the α value dropped to 0.18, implying a more compact structure, possibly due to increased homogeneity in the polymer chain. For the SCKP with a 25 : 75 feed ratio, the lowest α value of 0.11 was recorded, suggesting a highly compact coil structure. This aligns with the expectation that introducing DEGDA, a more hydrophobic monomer, would reduce solvation, leading to a tighter coil conformation. Overall, these results confirm the successful synthesis of SCKPs.

SCKPs exhibit tailorable LCST

We aim to synthesize SCKPs with an LCST lower or close to 37 °C to enable their use in cell encapsulation.[17,24] The LCST of representative SCKPs, synthesized using various monomer combinations and feed ratios, was investigated by measuring their optical transmittance in aqueous solutions. In deionized water at a concentration of 50 mg mL^{-1}, the SCKP composed of PEGDA575 and PEGDA700 at a 50 : 50 feed ratio exhibited an LCST of around 80 °C (Fig. 2a). As the feed ratio of PEGDA575 increased to 75, the LCST dropped to 65 °C, due to the higher hydrophobicity of the SCKP. When more hydrophobic DEGDA was introduced to replace PEGDA700, the LCST decreased further to 48 °C and 34 °C, respectively. The transition of SCKP solutions below and above the LCST was also visible to the naked eye. As shown in Fig. 2b, below the LCST, the SCKP solution appeared transparent and clear, while heating it above the LCST caused the solution to become a milky-white emulsion. The formation of particles was further observed under a microscope (Fig. 2c). We also examined the effect of DSDA and DMA on the LCST of SCKPs. Interestingly, when 20% DSDA and 10% DMA were incorporated, the LCST of the resulting SCKPs fell below 23 °C (Table S2). These findings confirm our hypothesis that by adjusting the monomer combinations and feed ratios, the LCST of the synthesized SCKPs can be fine-tuned across a wide temperature range.

Next, we explored the effects of concentration and solvent on the LCST of SCKPs in deionized water, PBS, and DMEM. Generally, the LCST in deionized water was higher than in PBS and DMEM (Fig. S5). For SCKPs composed of PEGDA575, DSDA, PEGDA700, and DMA at a 50 : 20 : 20 : 10 feed ratio, the LCST was 37 °C, 33 °C, and 33 °C at a concentration of

a

PEGDA700	PEGDA575	DEGDA	LCST (°C)
50	50	/	80±1.3
25	75	/	65±0.9
100	/	/	60±1.1
/	75	25	48±0.9
/	50	50	34±0.8

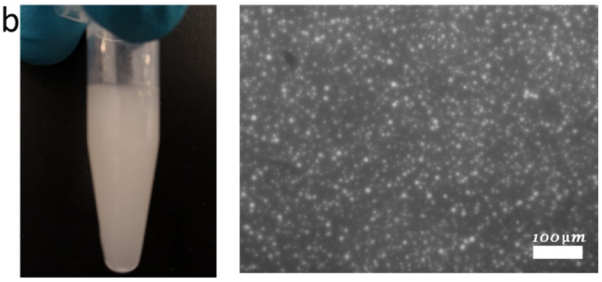

Fig. 2 SCKPs exhibit tailorable LCST. (a) LCST values of various SCKPs. (b) The SCKP composed of PEGDA575 and DEGDA at a 50 : 50 feed ratio becomes colloidal when heated to 37 °C. (c) Bright-field images of nanoparticles from the SCKP composed of PEGDA575 and DEGDA at a 50 : 50 feed ratio.

1 mg mL^{-1} in water, PBS, and DMEM, respectively. Increasing the SCKP concentration to 5 mg mL^{-1} reduced the LCST to 33 °C, 31 °C, and 29 °C. A further increase to 10 mg mL^{-1} led to LCST values of 32 °C, 30 °C, and 29 °C, respectively. SCKPs composed of PEGDA575 and DEGDA at a 50 : 50 feed ratio showed similar solvent- and concentration-dependent LCST behavior (Fig. S6). Notably, SCKPs with monomer combinations of PEGDA575, DEGDA, and DSDA at a 50 : 30 : 20 feed ratio or PEGDA575 and DEGDA at 50 : 50 exhibited LCSTs in the range of 29 °C to 37 °C (Tables S3 and S4), which makes them particularly promising for biomedical applications.

Cell encapsulation and toxicity

The tailorable thermo-responsiveness of SCKPs makes them highly suitable for cell encapsulation when heated above the LCST. First, we investigated the ability of SCKPs to form a hydrogel in the presence of the crosslinker HA-SH.[31] As illustrated in Fig. 3a, before adding HA-SH, the SCKP solution was a flowing liquid. However, after the addition of HA-SH, when the tube was inverted, no liquid flowed, indicating the formation of a transparent hydrogel *in situ*, validating the creation of a half interpenetrating polymer network (H-IPN). Next, SCKPs were incorporated into cell culture medium and incubated at 37 °C, where numerous particles adhered to the bottom of the cell culture plate. Despite this, the cell morphology remained unchanged and clearly visible, likely due to the high biocompatibility of the SCKPs. Upon adding HA-SH, gelation occurred *in situ*, fully encapsulating the cells while preserving their morphology (Fig. 3b). The gel formed by the SCKP and HA-SH was temperature-resistant, maintaining its structure both below and above the LCST. Interestingly, the gel's color became more vivid upon heating, providing a potential visual cue for temperature-induced structural changes.

Cell viability in the presence of SCKPs was assessed using alamarBlue assays.[32] Across concentrations ranging from 10 μg mL^{-1} to 100 μg mL^{-1}, the SCKPs generally exhibited high cell viability, though slight differences were observed between the polymers (Fig. 3c). As the SCKP concentration

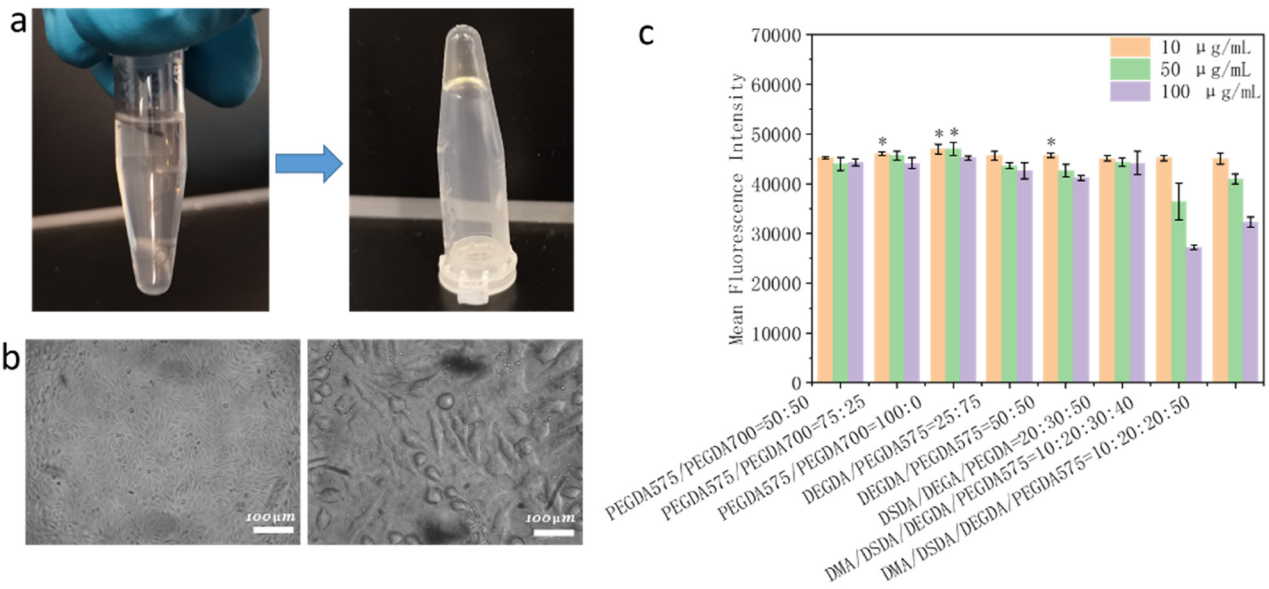

Fig. 3 SCKPs can crosslink with HA-SH to form a hydrogel and encapsulate cells *in situ*, ensuring high cell viability. (a) Images of the SCKP composed of PEGDA575 and DEGDA at a 50 : 50 feed ratio, shown before and after the addition of HA-SH. (b) Cells after incubation with the SCKP composed of PEGDA575 and DEGDA at a 50 : 50 feed ratio, before and after adding HA-SH. (c) Cell viability after incubation with the SCKP composed of PEGDA575 and DEGDA at concentrations of 10 μg mL^{-1}, 50 μg mL^{-1}, and 100 μg mL^{-1}. An asterisk (*) indicates superior cell viability compared to the SCKP composed of PEGDA575 and PEGDA700 at a 50 : 50 feed ratio.

increased, cell viability gradually decreased. For example, SCKPs composed of PEGDA575 and PEGDA700 at feed ratios of 50 : 50, 75 : 25, and 100 : 0, as well as SCKPs made of DEGDA and PEGDA575 at feed ratios of 25 : 75 and 50 : 50, showed a decline in cell viability as the concentration rose from 10 μg mL^{-1} to 100 μg mL^{-1}. This suggests that while SCKPs may exhibit concentration-dependent cytotoxicity, the effect is less pronounced at higher concentrations.

Conclusions

In this study, the RAFT polymerization method was used to successfully prepare SCKPs with thermal responsiveness. Its uniqueness mainly lies in the ability to design its low critical solution temperature (LCST) to be close to the human body's required temperature of 37 °C, by adjusting the specific monomer type and addition ratio, which is convenient for practical applications. Moreover, this setting makes the influence of temperature on it more precise and obvious, making it especially suitable for temperature-activated material functional scenarios in biomedicine and other fields. For example, it can be used in stem cell injections and controlled release processes, and it has potential for future diagnostic and therapeutic applications. These SCKPs can specifically produce interpenetrating network gels with hyaluronic acid (HA-SH), which contains mercapto groups. They form the core for preparing H-IPN hydrogels. During this period, it can efficiently package stem cells without causing significant toxicity. Therefore, it not only ensures their vitality but also creates conditions closer to the natural growth environment of cells. Compared with conventional polymer processes in the past, the RAFT method has outstanding advantages in accurately controlling the molecular weight, dispersity coefficient, and chain connectivity structure of polymers, ultimately enabling the mass production of SCKPs to achieve uniform and stable desired performance.

Conflicts of interest

The authors declare no conflicts of interest.

Data availability

All data included in this study are available upon request from the corresponding author.

Supplementary information (SI) is available. See DOI: https://doi.org/10.1039/d5ma00621j.

Acknowledgements

This work was funded by Capital's Funds for Health Improvement and Research (CFH 2024-2-20111), code: Z191100006619044. And also funded by the Beijing Hospitals Authority Clinical Medicine Development of Special Funding Support, code: ZYLX202134.

References

1 A. Anjum, *et al.*, Spinal Cord Injury: Pathophysiology, Multimolecular Interactions, and Underlying Recovery Mechanisms, *Int. J. Mol. Sci.*, 2020, **21**(20), 1–35.
2 X. Hu, *et al.*, Spinal cord injury: molecular mechanisms and therapeutic interventions, *Signal Transduction Targeted Ther.*, 2023, **8**(1), 245.
3 C. S. Ahuja, *et al.*, Traumatic spinal cord injury, *Nat. Rev. Dis. Primers*, 2017, **3**(1), 17018.
4 M. Karsy and G. Hawryluk, Modern Medical Management of Spinal Cord Injury, *Curr. Neurol. Neurosci. Rep.*, 2019, **19**(9), 65.
5 Z. Liu, *et al.*, High-dose methylprednisolone for acute traumatic spinal cord injury: A meta-analysis, *Neurology*, 2019, **93**(9), e841–e850.
6 R. A. Barker, M. Götz and M. Parmar, New approaches for brain repair—from rescue to reprogramming, *Nature*, 2018, **557**(7705), 329–334.
7 E. Kronvall, F. T. Sayer and O. G. Nilsson, Methylprednisolone in the treatment of acute spinal cord injury has become more and more questioned, *Lakartidningen*, 2005, **102**(24–25), 1887–1890.
8 P. J. Jongen, *et al.*, Patient-reported adverse effects of high-dose intravenous methylprednisolone treatment: a prospective web-based multi-center study in multiple sclerosis patients with a relapse, *J. Neurol.*, 2016, **263**(8), 1641–1651.
9 M. C. Caruso, *et al.*, Lessons learned from administration of high-dose methylprednisolone sodium succinate for acute pediatric spinal cord injuries, *J. Neurosurg. Pediatr.*, 2017, **20**(6), 567–574.
10 N. Xiao and Q. T. Le, Neurotrophic Factors and Their Potential Applications in Tissue Regeneration, *Arch. Immunol. Ther. Exp.*, 2016, **64**(2), 89–99.
11 Y. El Ouaamari, *et al.*, Neurotrophic Factors as Regenerative Therapy for Neurodegenerative Diseases: Current Status, Challenges and Future Perspectives, *Int. J. Mol. Sci.*, 2023, **24**(4), 1–24.
12 M. Konno, *et al.*, Adipose-derived mesenchymal stem cells and regenerative medicine, *Dev., Growth Differ.*, 2013, **55**(3), 309–318.
13 Z. Si, *et al.*, Adipose-derived stem cells: Sources, potency, and implications for regenerative therapies, *Biomed. Pharmacother.*, 2019, **114**, 108765.
14 B. A. Bunnell, Adipose Tissue-Derived Mesenchymal Stem Cells, *Cells*, 2021, **10**(12), 1–7.
15 Y. Qin, *et al.*, An Update on Adipose-Derived Stem Cells for Regenerative Medicine: Where Challenge Meets Opportunity. Advanced, *Science*, 2023, **10**(20), 2207334.
16 C. H. Pinheiro, *et al.*, Local injections of adipose-derived mesenchymal stem cells modulate inflammation and increase angiogenesis ameliorating the dystrophic phenotype in dystrophin-deficient skeletal muscle, *Stem Cell Rev. Rep.*, 2012, **8**(2), 363–374.
17 T. Liu, *et al.*, Advances of adipose-derived mesenchymal stem cells-based biomaterial scaffolds for oral and maxillofacial tissue engineering, *Bioact. Mater.*, 2021, **6**(8), 2467–2478.

18 H. Cao, *et al.*, Current hydrogel advances in physicochemical and biological response-driven biomedical application diversity, *Signal Transduction Targeted Ther.*, 2021, **6**(1), 426.
19 I. M. El-Sherbiny and M. H. Yacoub, Hydrogel scaffolds for tissue engineering: Progress and challenges, *Glob. Cardiol. Sci. Pract.*, 2013, **2013**(3), 316–342.
20 X. Li and J. P. Gong, Design principles for strong and tough hydrogels, *Nat. Rev. Mater.*, 2024, **9**(6), 380–398.
21 Q. Xu, *et al.*, Bacteria-Resistant Single Chain Cyclized/Knotted Polymer Coatings, *Angew. Chem., Int. Ed.*, 2019, **58**(31), 10616–10620.
22 F. M. Haque and S. M. Grayson, The synthesis, properties and potential applications of cyclic polymers, *Nat. Chem.*, 2020, **12**(5), 433–444.
23 S. Forg, *et al.*, Copolymerization Kinetics of Dopamine Methacrylamide during PNIPAM Microgel Synthesis for Increased Adhesive Properties, *Langmuir*, 2022, **38**(17), 5275–5285.
24 Y. Yuan, *et al.*, Thermoresponsive polymers with LCST transition: synthesis, characterization, and their impact on biomedical frontiers, *RSC Appl. Polym.*, 2023, **1**(2), 158–189.
25 C. Barner-Kowollik, *et al.*, Reversible Addition Fragmentation Chain Transfer (RAFT) Polymerization: Mechanism, Process and Applications, in Encyclopedia of Radicals in Chemistry, *Biol. Mater.*, 2012, 493–502.
26 G. Moad, A Critical Assessment of the Kinetics and Mechanism of Initiation of Radical Polymerization with Commercially Available Dialkyldiazene Initiators, *Prog. Polym. Sci.*, 2019, **88**, 130–188.
27 S. S. Rane and P. Choi, Polydispersity Index: How Accurately Does It Measure the Breadth of the Molecular Weight Distribution?, *Chem. Mater.*, 2005, **17**(4), 926.
28 C. Auch, M. Harms and K. Mäder, How changes in molecular weight and PDI of a polymer in amorphous solid dispersions impact dissolution performance, *Int. J. Pharm.*, 2019, **556**, 372–382.
29 E. J. Singley, *et al.*, Determination of Mark-Houwink parameters for poly(N-vinylformamide), *J. Polym. Sci., Part A: Polym. Chem.*, 1997, **35**(12), 2533–2534.
30 Y. Lu, *et al.*, Synthesis of structurally controlled hyperbranched polymers using a monomer having hierarchical reactivity, *Nat. Commun.*, 2017, **8**(1), 1863.
31 Z. Luo, *et al.*, Modification and crosslinking strategies for hyaluronic acid-based hydrogel biomaterials, *Smart Med.*, 2023, **2**(4), e20230029.
32 P. Kumar, A. Nagarajan and P. D. Uchil, Analysis of Cell Viability by the alamarBlue Assay, *Cold Spring Harb Protoc*, 2018, **2018**(6), 462–464.